



Citation for published version:

Zhong, CJ, Hu, XL, Yang, XL, Gan, HQ, Yan, KC, Shu, FT, Wei, P, Gong, T, Luo, PF, James, TD, Chen, ZH, Zheng, YJ, He, XP & Xia, ZF 2022, 'Metabolically Specific In Situ Fluorescent Visualization of Bacterial Infection on Wound Tissues', *ACS Applied Materials and Interfaces*, vol. 14, no. 35, pp. 39808-39818.
<https://doi.org/10.1021/acsami.2c10115>

DOI:

[10.1021/acsami.2c10115](https://doi.org/10.1021/acsami.2c10115)

Publication date:

2022

Document Version

Peer reviewed version

[Link to publication](#)

This document is the Accepted Manuscript version of a Published Work that appeared in final form in *ACS Appl. Mater. Interfaces*, copyright © American Chemical Society after peer review and technical editing by the publisher. To access the final edited and published work see <https://doi.org/10.1021/acsami.2c10115>

University of Bath

Alternative formats

If you require this document in an alternative format, please contact:
openaccess@bath.ac.uk

General rights

Copyright and moral rights for the publications made accessible in the public portal are retained by the authors and/or other copyright owners and it is a condition of accessing publications that users recognise and abide by the legal requirements associated with these rights.

Take down policy

If you believe that this document breaches copyright please contact us providing details, and we will remove access to the work immediately and investigate your claim.

Metabolically Specific in-situ Fluorescent Visualization of Bacterial Infection on Wound Tissues

Chen-Jian Zhong,^{†a,c} Xi-Le Hu,^{†b} Xiao-Lan Yang,^{†a,c,d} Hui-Qi Gan,^b Kai-Cheng Yan,^b Fu-Ting Shu,^c
Pei Wei,^a Teng Gong,^a Peng-Fei Luo,^c Tony D. James,^{e,f} Zhao-Hong Chen,^{*a} Yong-Jun Zheng,^{*c}
Xiao-Peng He,^{*b,g,h} and Zhao-Fan Xia^{*a,c}

^aDepartment of Burn Surgery and Wound Repair, Fujian Burn Medical Center, Fujian Provincial Key Laboratory of Burn and Trauma, Fujian Medical University Union Hospital, Fuzhou 350001, Fujian, P. R. China

^bKey Laboratory for Advanced Materials and Joint International Research Laboratory of Precision Chemistry and Molecular Engineering, Feringa Nobel Prize Scientist Joint Research Center, School of Chemistry and Molecular Engineering, Frontiers Center for Materiobiology and Dynamic Chemistry, East China University of Science and Technology, 130 Meilong Rd, Shanghai 200237, P. R. China

^cDepartment of Burn Surgery, the First Affiliated Hospital of Naval Medical University, Shanghai 200433, P. R. China; Research Unit of key techniques for treatment of burns and combined burns and trauma injury, Chinese Academy of Medical Sciences

^dDepartment of Burn Surgery and Wound Repair, Quanzhou First Hospital Affiliated to Fujian Medical University, Quanzhou 362001, Fujian, China

^eDepartment of Chemistry, University of Bath, Bath, BA27AY, UK

^fSchool of Chemistry and Chemical Engineering, Henan Normal University, Xinxiang 453007, P. R. China

^gThe International Cooperation Laboratory on Signal Transduction, Eastern Hepatobiliary Surgery Hospital, Shanghai 200438, China

^hNational Center for Liver Cancer, Shanghai 200438, China

[‡]Equal contribution

Keywords: Folate, Bacteria, Fluorescence Imaging, Wound Infection, Metabolism

ABSTRACT: The ability to effectively detect bacterial infection in human tissues is important for the timely treatment of the infection. However, traditional techniques fail to visualize bacterial species adhered to host cells *in-situ* in a target-specific manner. Dihydropteroate synthase (DHPS) exclusively exists in bacterial species and metabolically converts *p*-aminobenzoic acid (PABA) to folic acid (FA). By targeting this bacterium-specific metabolism, we have developed a fluorescent imaging probe, **PABA-DCM**, based on the conjugation of PABA with a long-wavelength dicyanomethylene 4*H*-pyran (**DCM**) fluorophore. We confirmed that the probe can be used in the synthetic pathway of a broad spectrum of gram-positive and negative bacteria, resulting in a significantly extended retention time in bacterial over mammalian cells. We validated that DHPS catalytically introduces a dihydropteridine group to the amino end of the PABA motif of **PABA-DCM**, and the resulting adduct leads to an increase in the FA levels of bacteria. We also constructed a hydrogel dressing containing **PABA-DCM** and graphene oxide (GO), termed **PABA-DCM@GO** that achieves target-specific fluorescence visualization of bacterial infection on the wounded tissues of mice. Our research paves the way for the development of fluorescent imaging agents that target species-conserved metabolic pathways of microorganisms for the *in-situ* monitoring of infections in human tissues.

Introduction

Wound infections can cause progressive inflammation, destroy soft tissues in the infected area and inhibit wound healing.¹ The World Health Organization estimates that by 2050, wound infections caused by bacteria will result in 10 million deaths annually.² The ability to quickly visualize bacterial species on wound tissues *in-situ* is important as an early warning of infection, the timely eradication of bacteria, and the monitoring of subsequent therapeutic treatments. However, current clinical methods including wound swab and biopsy (the biopsied specimens are typically used for microbiological analyses and gene sequencing) are unable to achieve this goal since they are unable to specifically visualize bacterial infection on wounded human tissues *in-situ*.^{3,4}

Small-molecule based fluorescent probes, owing to their ease in preparation and implementation, high sensitivity, low cost, and capability for spatiotemporal monitoring of biologically important biomarkers, have attracted the interest of both academic and industrial groups over the past few decades.⁵⁻¹¹ Recently, some elegant small-molecule fluorescent probes have been developed for bacterial detection by specifically targeting a diverse range of extracellular and intracellular biomarkers.¹¹⁻²³ The targeted extracellular elements include lipopolysaccharides,¹⁴ transmembrane glycoproteins,¹⁶ negatively charged teichoic acids,¹⁷ and cell-wall peptidoglycans.¹⁸ In addition, the intracellular biomarkers that can be targeted for the detection of bacterial species include nucleic acids, functional enzymes, and other signaling molecules.¹⁹⁻²¹ However, to the best of our knowledge, small-molecule fluorescent probes capable of targeting a dynamic metabolic pathway that is highly conserved in a broad spectrum of bacterial species have yet to be developed.

While mammals are capable of direct uptake of folic acids (FAs) through FA receptors expressed in nearly all types of mammalian cells,²⁴ bacteria produce FAs from *p*-aminobenzoic acid (PABA).²⁵ In a growing environment, bacteria use PABA and dihydropterin diphosphate (DHPPP) to synthesize dihydropteroate (DHP) under the catalysis of dihydropteroate synthase (DHPS).²⁶ Then, DHP is further metabolically converted to tetrahydrofolate (THF), which is indispensable in the survival of bacteria, due to its vital role in the synthesis of nucleic acids and proteins.²⁵ Considering that the DHPS-dependent FA synthetic pathway exclusively exists in bacterial species, we sought to develop a fluorescent probe that specifically targets the DHPS-mediated dynamic signaling pathway for the selective visualization of bacteria over mammalian cells.

Here, we report the construction of the fluorescent imaging probe (**PABA-DCM**) based on the simple conjugation of PABA with a long-wavelength fluorescent dye, dicyanomethylene 4*H*-pyran (**DCM**), using the Cu(I)-catalyzed azide-alkyne cycloaddition “click” reaction. The PABA motif of the probe can be specifically exploited by bacteria in the DHPS-dependent FA synthetic pathway to produce a DHP-coupled **DCM** intermediate, which is subsequently degraded and used to generate FA (Figure 1a). This metabolic action results in a prolonged retention of **PABA-DCM** in bacterial species that exclusively expresses DHPS over mammalian cells. In contrast, **DCM** without PABA modification does not participate in the DHPS-dependent FA synthetic pathway and is therefore quickly excreted by bacteria (Figure 1b). We also constructed a hydrogel dressing consisting of **PABA-DCM** with graphene oxide (GO), creating **PABA-DCM@GO** for the target-specific fluorescence visualization of bacterial infection on the wounded tissues of mice (Figure 1c).

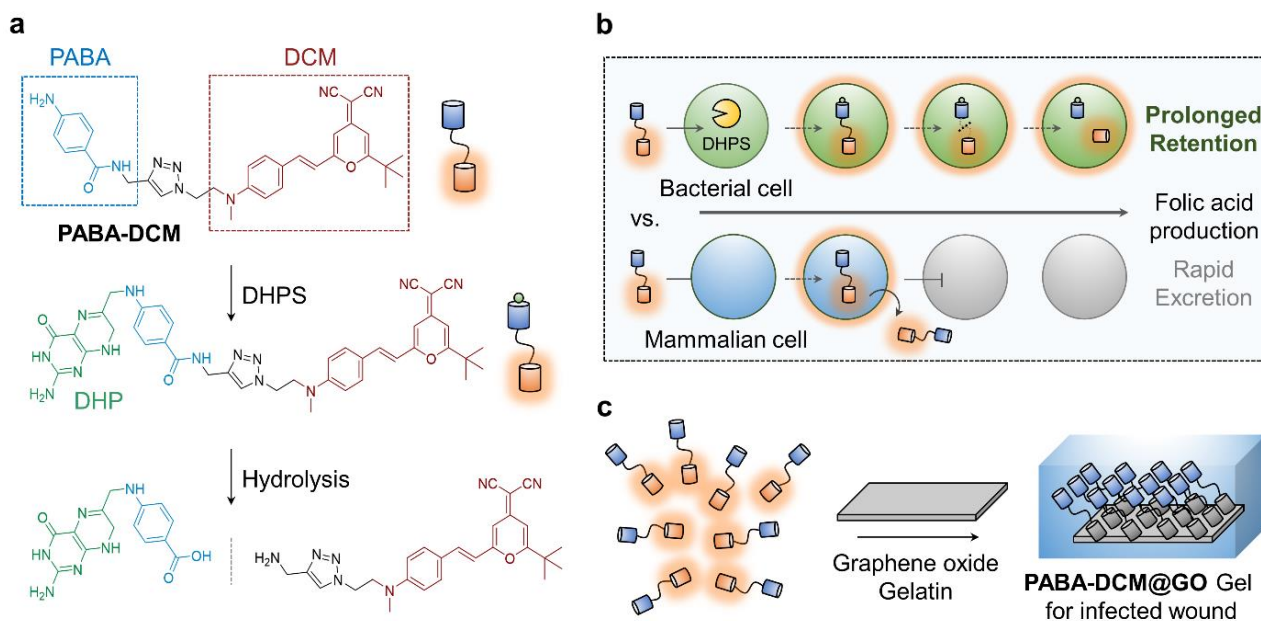


Figure 1. Schematic illustration of the metabolically-selective fluorescence imaging of bacteria using **PABA-DCM**. (a) Structure of **PABA-DCM** and its specific structural transformation mediated by enzymes selectively expressed in bacteria. (b) Schematic illustration of the mechanism by which bacteria-specific *in-situ* imaging is achieved by the probe. After internalization by bacterial species that highly expresses 7,8-dihydropteroate synthase (DHPS), **PABA-DCM** is used by the DHPS-dependent biosynthetic pathway, thereby resulting in a prolonged retention time intracellularly. However, when internalized by mammalian cells that lack DHPS expression, the probe is quickly excreted by the cells. (c) Self-assembly between **PABA-DCM** and graphene oxide (GO) producing a **PABA-DCM/GO** hydrogel for metabolically visualizing bacterial infection on the wounded tissues of mice. PABA, p-Aminobenzoic acid. DCM, dicyanomethylene 4*H*-pyran.

Results and discussion

Synthesis of PABA-DCM. A known long-wavelength **DCM** dye²⁷ was used for coupling with PABA via the CuAAC click reaction (Scheme S1). Amidation between PABA (**a**) and 2-propynylamine (**b**) produced the propargyl PABA intermediate **c**, which then underwent a cycloaddition reaction with a known azido **DCM** derivative (**d**)²⁸ to produce the desired triazole-linked **PABA-DCM** probe (Figure 1a). **DCM** without PABA modification was used as a control probe.

Metabolic retention of PABA-DCM in bacterial species through the DHPS-mediated FA metabolic pathway. To produce FA, bacteria internalize PABA as a raw material *via* the DHPS-dependent metabolic pathway, while, FA is directly obtained from the diet for mammals.^{24,25} Through an initial multiple sequence alignment, we found that the *folP* gene (Figure S1) as well as the amino acid sequences (Figure S2) encoding DHPS are present in several bacterial species,^{29,30} and a subsequent homology comparison shows that DHPS expression is highly conserved in bacteria over mice and humans (Table 1).

Table 1. Sequence alignment of different species.^a

		Identity to <i>S. aureus</i> (%)	
		<i>folP</i>	DHPS
Bacterial species			
Aerobic and facultative anaerobic Gram-positive bacteria			
1	<i>Staphylococcus aureus</i> (<i>S. aureus</i>)	100.00	100.00
2	<i>Staphylococcus aureus</i> (strain MSSA476)	99.38	95.51
3	<i>Staphylococcus aureus</i> (strain MRSA252)	95.40	100.00
4	<i>Staphylococcus epidermidis</i> (strain ATCC 35984 / RP62A)	74.00	76.40
5	<i>Staphylococcus haemolyticus</i>	74.75	74.16
6	<i>Enterococcus faecalis</i> (strain ATCC 700802 / V583)	48.96	34.88

7	<i>Enterococcus faecium</i>	42.36	32.69
8	<i>Streptococcus pyogenes</i>	54.05	44.16
9	<i>Streptococcus pneumoniae</i>	46.03	36.88

Special Gram-positive pathogen

10	<i>Mycobacterium tuberculosis</i> (strain ATCC 25618 / H37Rv)	42.12	37.74
11	<i>Mycobacterium leprae</i> (strain TN)	44.03	37.17

Aerobic and facultative anaerobic Gram-negative bacteria

12	<i>Pseudomonas aeruginosa</i>	42.26	36.19
13	<i>Acinetobacter baumannii</i>	47.56	34.77
14	<i>Escherichia coli</i> (strain K12)	46.28	36.88
15	<i>Enterobacter cloacae</i>	44.74	36.12
16	<i>Enterobacter cloacae subsp. Cloacae</i>	44.62	36.12
17	<i>Klebsiella pneumoniae</i>	43.97	35.74
18	<i>Stenotrophomonas maltophilia</i> (strain K279a)	40.71	35.04
19	<i>Aeromonas hydrophila subsp. Hydrophila</i>	41.18	33.97
20	<i>Neisseria gonorrhoeae</i>	45.07	36.82
21	<i>Neisseria meningitidis serogroup B</i> (strain MC58)	45.36	37.98

Anaerobic bacteria

22	<i>Clostridium perfringens</i>	57.25	47.47
----	--------------------------------	-------	-------

Homo sapiens (human)

— —

Mice

— —

a. Homology comparison of cDNA (*folP*) and amino acids of *S. aureus* encoding DHPS (dihydropteroate synthase) with other pathogenic bacteria, human and mice in the UniProtKB and EMBL-EBI database using the multiple sequence alignment tool Clustal Omega. *folP* and DHPS exist in all surveyed bacterial species, but not in humans and mice.

To begin with, a variety of Gram-positive bacteria including *Staphylococcus aureus* ATCC 12600 (*S. aureus*) and *Enterococcus faecalis* ATCC19433 (*E. faecalis*), and Gram-negative bacteria including *Acinetobacter baumannii* ATCC 19606 (*A. baumannii*), *Escherichia coli* ATCC 11775 (*E. coli*) and *Pseudomonas aeruginosa* ATCC 10145 (*P. aeruginosa*) were used for imaging assays with **PABA-DCM** using a confocal laser-scanning microscope (CLSM) (Figure 2). **DCM** was used as control under the same conditions. We detected a strong **PABA-DCM** fluorescence in all bacterial species used for imaging, which overlapped well with that of SYTO-9 green (a known staining agent for nucleic acids) (Figure 2a). However, the fluorescence of **DCM** was almost absent in all bacteria tested (Figure 2b). This preliminary result suggests that **PABA-DCM** is more selective for bacterial imaging than the unmodified **DCM** equivalent.

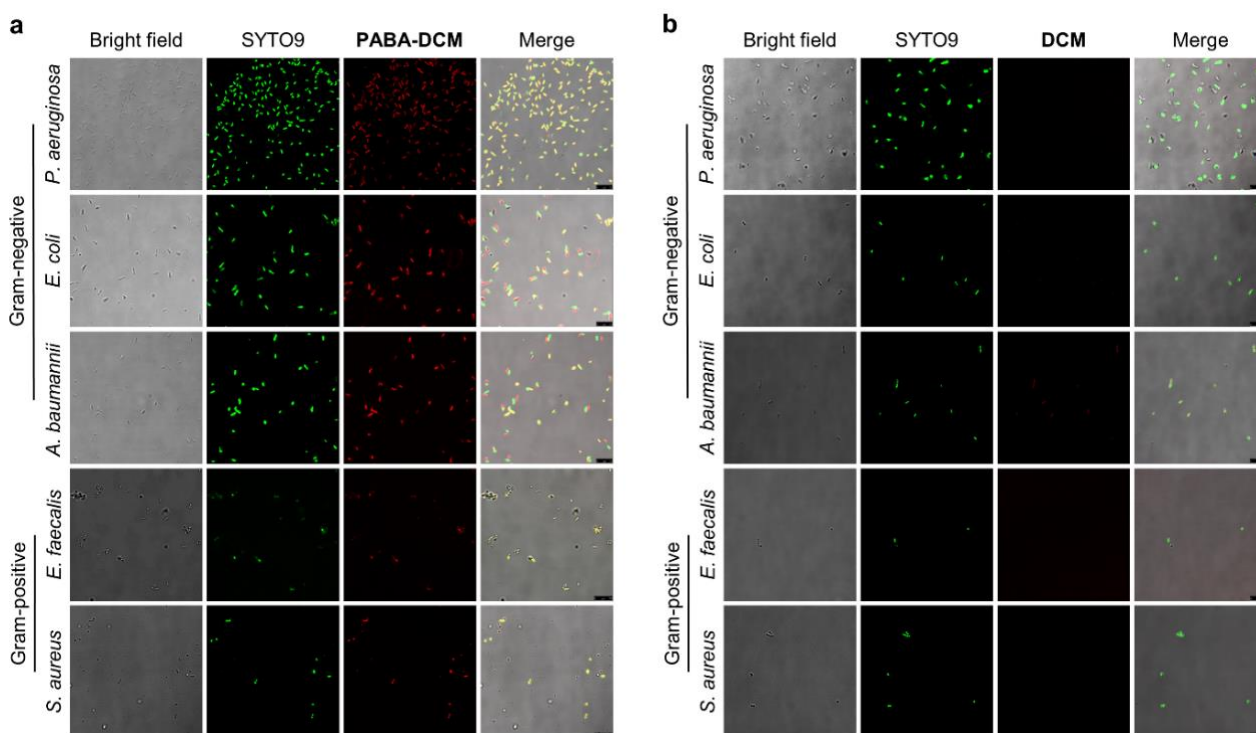


Figure 2. PABA-DCM specifically accumulated in a variety of bacteria. Representative fluorescence images of different Gram-negative bacterial strains including *Pseudomonas aeruginosa*

(*P. aeruginosa*) ATCC 10145, *Escherichia coli* (*E. coli*) ATCC 11775, and *Acinetobacter baumannii* (*A. baumannii*) ATCC 19606, and Gram-positive bacterial strains including *Enterococcus faecalis* (*E. faecalis*) ATCC 19433 and *Staphylococcus aureus* (*S. aureus*) ATCC 12600 (10^6 CFU mL⁻¹) incubated with (a) **PABA-DCM** (10 μ M) and (b) **DCM** (10 μ M) for 2 h by a confocal-scanning laser microscope. SYTO-9 (1 μ M) was used to stain bacterial nucleic acids. **PABA-DCM** and **DCM** channel: $\lambda_{\text{ex}} = 460$ nm, $\lambda_{\text{em}} = 630$ nm; SYTO-9 channel: $\lambda_{\text{ex}} = 485\text{-}486$ nm, $\lambda_{\text{em}} = 498\text{-}501$ nm. Scale bars: 7.5 μ m.

Then, a time-dependent fluorescence imaging assay was carried out. As such, both **PABA-DCM** and **DCM** were incubated with *P. aeruginosa* as a model bacterial strain (Figure S3). We observed that both dyes exhibited a similar level of fluorescence at 0.5 h, and the fluorescence of **DCM** began to decline sharply from 1.0 h to 2.0 h (Figures S3a and S3b). In contrast, the intracellular fluorescence of **PABA-DCM** continued to enhance from 1.0 h to 1.5 h, and decreased slightly at 2.0 h. The fluorescence intensity of **PABA-DCM** was determined to be *ca.* 6.5-fold larger than that of **DCM** after 2 h of incubation, suggesting that the former accumulates and is retained in bacteria much more effectively than the latter.

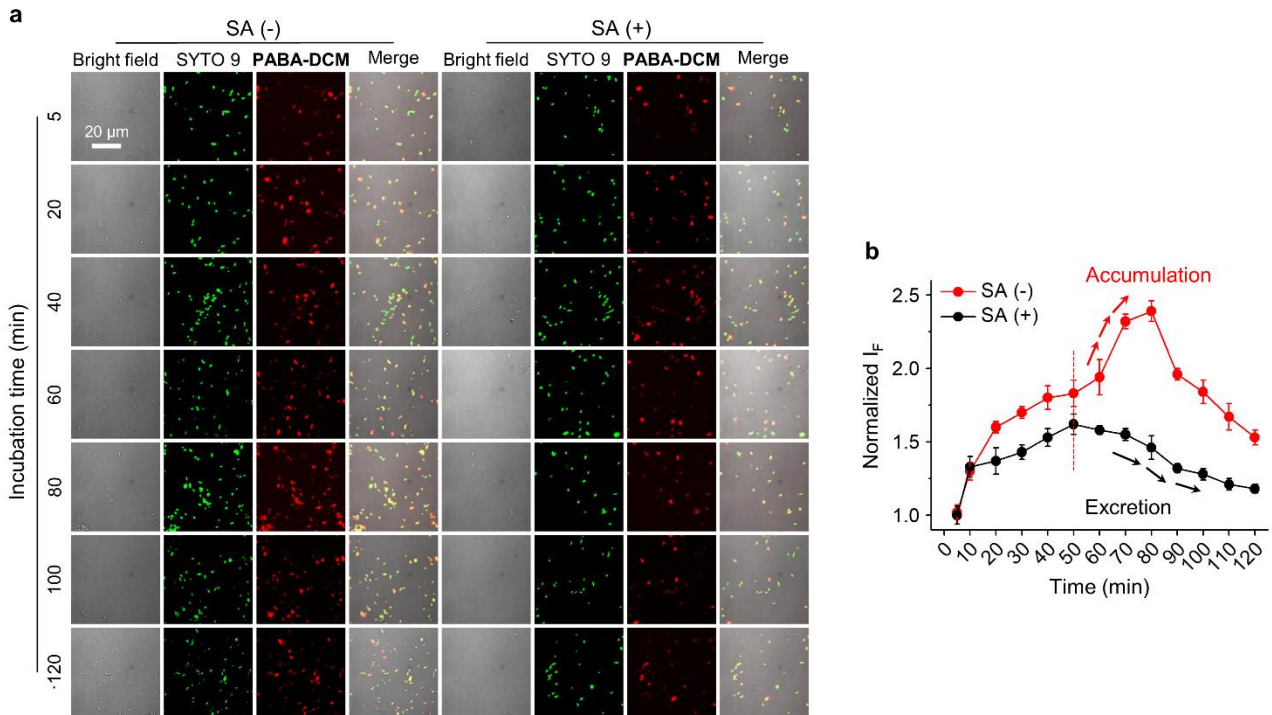


Figure 3. Time-dependent fluorescence imaging of a representative Gram-positive bacterial strain, *S. aureus*. (a) Representative fluorescence images of *Staphylococcus aureus* ATCC 12600 (*S. aureus*) (10^6 CFU mL⁻¹) without and with pretreatment of SA (Sulfanilamide, 1000 μ M), followed by incubation with **PABA-DCM** (10 μ M) for 0-120 min by a confocal-scanning laser microscope. (b) Quantification of **PABA-DCM** fluorescence shown in the images of panel (a) (for complete fluorescence images, see Fig. S4). SYTO-9 (1 μ M) was used to stain bacterial nucleic acids. **PABA-DCM** and **DCM** channel: $\lambda_{\text{ex}} = 460$ nm, $\lambda_{\text{em}} = 630$ nm; SYTO-9 channel: $\lambda_{\text{ex}} = 485\text{-}486$ nm, $\lambda_{\text{em}} = 498\text{-}501$ nm. Scale bars: 7.5 μ m.

To validate that the prolonged retention of **PAPA-DCM** is dependent on the DHPS-mediated FA metabolic pathway, a series of other experiments were performed. We first evaluated whether the presence of a known DHPS inhibitor, sulfanilamide (SA), would competitively reduce the accumulation of **PAPA-DCM** in bacteria. As such, a pair of Gram-positive (*S. aureus*) and negative

P. aeruginosa) bacterial strains was used. Bacteria were pre-treated with SA (SA (+)), incubated with the probe, and then the resulting fluorescence images were recorded at 5 min, 10 min, and then every 10 min for 120 min; those without pre-treatment with SA were used as control (SA (-)) (Figures 3 and 4). We observed that **PABA-DCM** exhibited a gradual fluorescence enhancement in *S. aureus* from 5 min to 40 min in both SA (+) and SA (-) groups (Figures 3a and 3b, Figure S4). However, at 50 min, while the fluorescence of **PABA-DCM** continued to increase in the SA (-) group, it began to drop for the SA (+) group. In the SA (+) group, the fluorescence did not decline until 80 min, and at the final time point (120 min), the fluorescence of **PABA-DCM** was significantly stronger in the SA (-) group than that in the SA (+) group.

A similar trend in fluorescence variation was also observed for the Gram-negative bacterial stain (*P. aeruginosa*) after pre-treatment with SA (Figures 4a and 4b, Figure S5). A sharp fluorescence decrease was observed for the probe from 40 min in the SA (+) group, while the fluorescence enhancement of **PABA-DCM** continued up to 80 min. These results suggest that the inhibition of DHPS activity suppresses the fluorescence of **PABA-DCM** in bacteria. We also evaluated the time-dependent fluorescence changes of **PABA-DCM** in human skin cells including human keratinocyte (HaCaT) human foreskin fibroblast (HFF) and human microvascular endothelial (HMEC) cells without endogenous DHPS expression (Figure S6). The results indicated that the probe was effectively internalized by the cells and began to be excreted quickly after 10 min (Figures S6a and S6b). At 60 min, almost no fluorescence of the probe was observed in the human cells. This observation is akin to that seen for SA-treated bacterial cells, corroborating the importance of DHPS for intracellular retention of **PABA-DCM**.

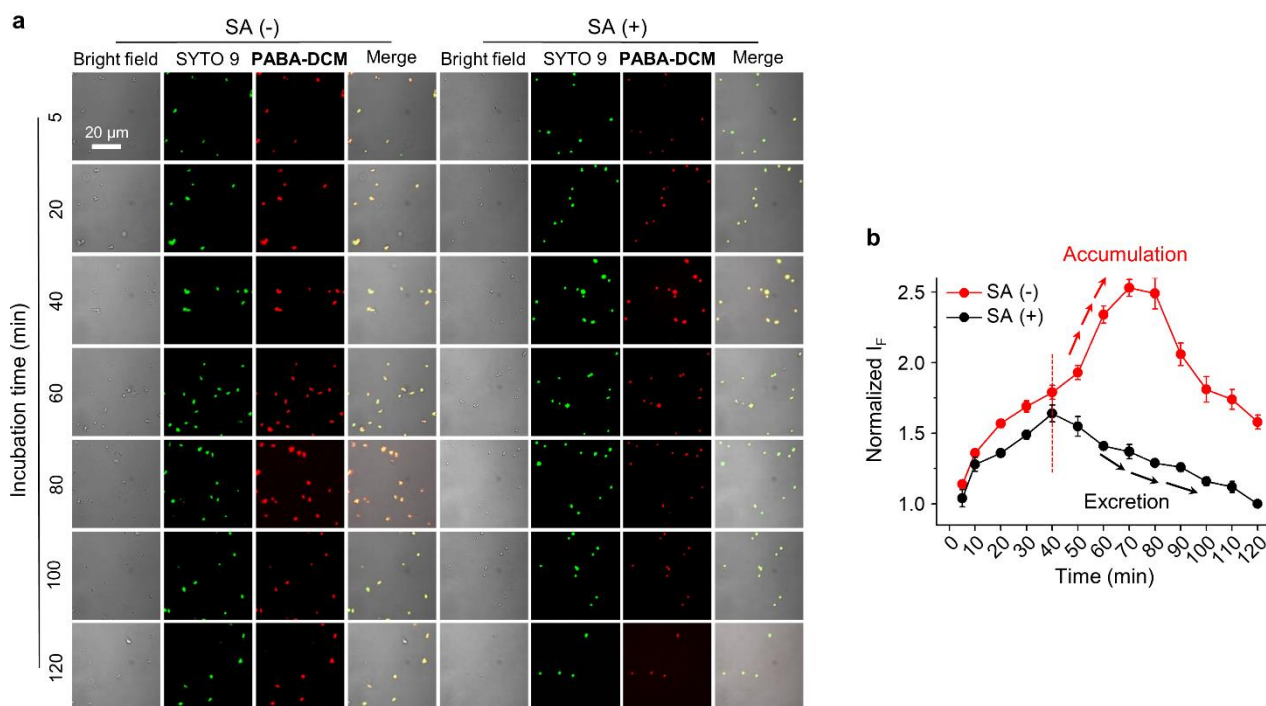


Figure 4. Time-dependent fluorescence imaging of a representative Gram-negative bacterial strain, *P. aeruginosa*. (a) Representative fluorescence images of *Pseudomonas aeruginosa* ATCC 10145 (*P. aeruginosa*) (10^6 CFU mL⁻¹) without and with pretreatment of SA (Sulfanilamide, 1000 μM), followed by incubation with **PABA-DCM** (10 μM) for 0-120 min by a confocal-scanning laser microscope. (b) Quantification of **PABA-DCM** fluorescence shown in the images of panel (a) (for complete fluorescence images, see Fig. S5). SYTO-9 (1 μM) was used to stain bacterial nucleic acids. **PABA-DCM** and DCM channel: $\lambda_{\text{ex}} = 460$ nm, $\lambda_{\text{em}} = 630$ nm; SYTO-9 channel: $\lambda_{\text{ex}} = 485\text{-}486$ nm, $\lambda_{\text{em}} = 498\text{-}501$ nm. Scale bars: 7.5 μm.

To better illustrate the mechanism of action for the prolonged retention of **PABA-DCM** in bacteria, high-performance liquid chromatography (HPLC) and mass spectroscopy (MS) were employed. We determined that the concentration of **DCM** decreased quickly in *P. aeruginosa* over time, and almost no signal was detectable at 2.0 h (Fig. S7b). Nevertheless, **PABA-DCM** was found to diminish much

more slowly in bacterial cells than **DCM**, with a recovery rate of 37.9% at 2.0 h (Fig. S7a). MS was used to characterize the structural transformation of **PABA-DCM** in bacteria (Fig. S8). In the bacterial lysate after being incubated with **PABA-DCM** for 2 h, we observed a MS signal that could be assigned to DHP ($[m + K]$ m/z 353.2650) as well as that to an amino triazolyl **DCM** metabolite ($[m + Na]$ m/z 478.1650). Considered in concert, we deduce that the substantially stronger fluorescence of **PABA-DCM** than **DCM** in bacterial cells after 2 h of incubation was the result of the continued utilization of **PABA-DCM** by the DHPS-mediated pathway, through which it was being converted into metabolic products, which resulted in an extended intracellular retention of the fluorescent **DCM** residue.

The above-results corroborate our hypothesis that **PABA-DCM** participates in the FA synthetic pathway with the addition of a dihydropteridine group to the amino end of the probe as the initial step (Figure 1a and Figure 5a).^{31, 32} Subsequently, the DHP-DCM adduct of the probe is hydrolyzed intracellularly to produce DHP and a **DCM**-containing fluorescent residue; the former is used for FA accumulation in bacteria, and the latter was eventually metabolically degraded to produce the residual **DCM** species as detected in the MS spectrum (Figure S8). Indeed, using an enzyme-linked immunosorbent assay (ELSA), we determined that all 5 bacteria used in this study produced a similar level of FA after incubation with **PABA-DCM**, comparing to that with PABA (Figure 5b). This confirms that **PABA-DCM** is used by the DHPS-dependent metabolic pathway for the generation of FA in bacteria.

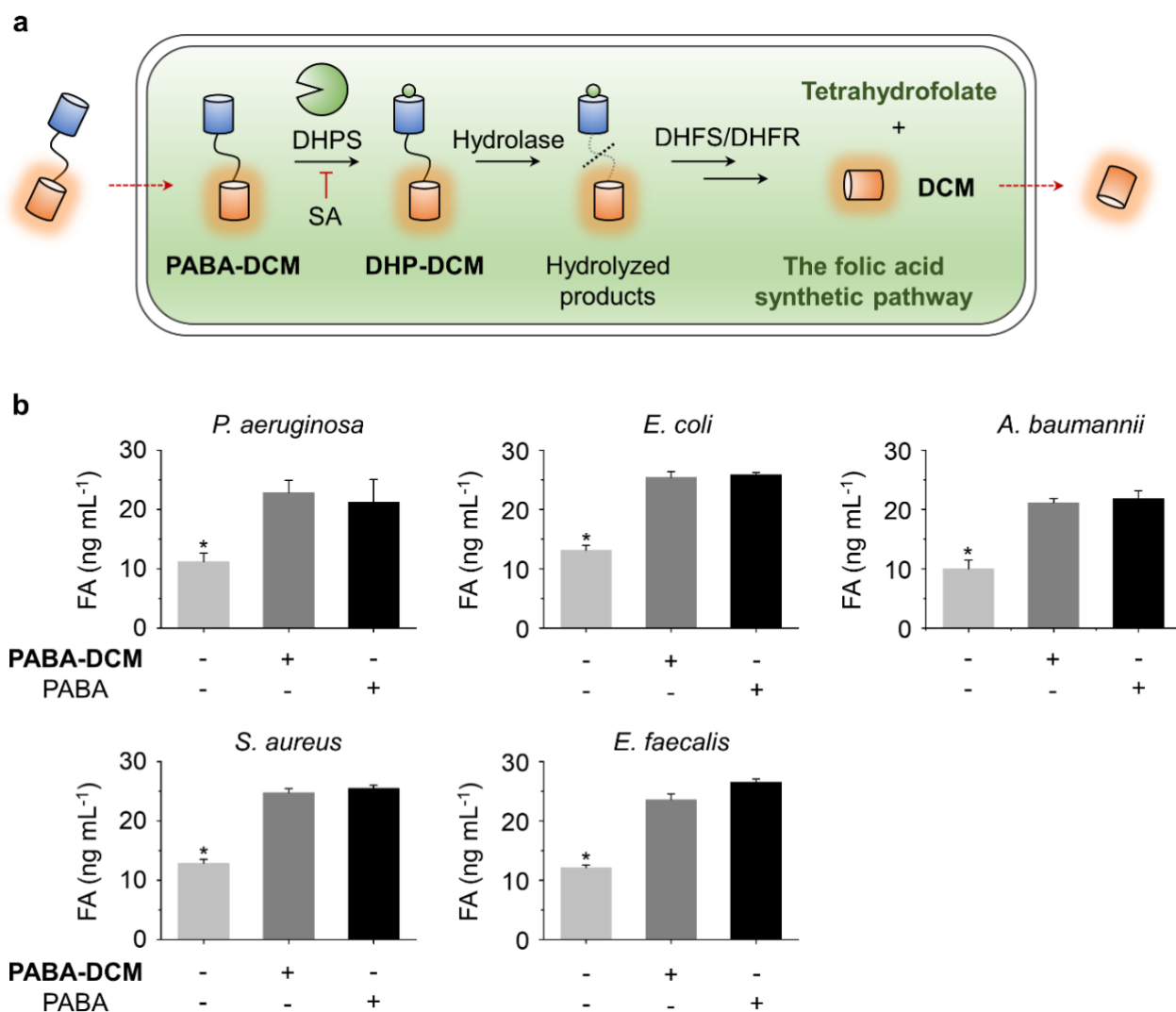


Figure 5. PABA-DCM upregulates folic acid level in different bacteria. (a) Schematic illustration of the metabolic pathway of **PABA-DCM** to produce tetrahydrofolates in bacteria mediated by 7,8-dihydropteroate synthase (DHPS). DHPS catalyzes the addition of a dihydropteridine group to the amino end of **PABA-DCM** producing **DHP-DCM**. After being hydrolyzed by intracellular hydrolases, the sequential catalytic transformation of the resulting DHP by dihydrofolate synthase (DHFS) and dihydrofolate reductase (DHFR) leads to the production of tetrahydrofolates. However, the presence of sulfanilamide (SA) competitively suppresses the activity of DHPS. (b) Quantification of folic acid (FA) concentration in different bacteria including *Pseudomonas aeruginosa* (*P. aeruginosa*) ATCC

10145, *Escherichia coli* (*E. coli*) ATCC 11775, *Acinetobacter baumannii* (*A. baumannii*) ATCC 19606, *Enterococcus faecalis* (*E. faecalis*) ATCC 19433 and *Staphylococcus aureus* (*S. aureus*) ATCC 12600 (10^6 CFU mL⁻¹) after treatment with **PABA-DCM** (10 μ M) for 2 h; PABA was used as a positive control. S. D. means standard deviation (n = 3); * $P < 0.05$.

Binding mode between PABA-DCM and DHPS simulated using molecular docking. DHPS exhibits a classical α/β TIM barrel structure, and DHPPP binds into a deep and highly conserved pocket of the β barrel of DHPS. While, the PABA binding site is located to the edge of the barrel.³³ To explore the binding mechanism of **PABA-DCM** with DHPS, we used the SwissDock's online molecular docking webserver to predict the potential binding modes using DHPS models from the five bacteria evaluated above.³⁴ PABA and SA were also used as controls for the docking calculations (Fig. S9). In general, the poses obtained from docking indicated that **PABA-DCM** and SA interact with DHPS from all the representatively selected bacterial strains in a manner similar to the resolved crystal structure of PABA with DHPS (PDB code: 5U10).³⁵ For instance, in *Pa*DHPS (*Pseudomonas aeruginosa* dihydropteroate synthase), the para aminophenyl groups of **PABA-DCM** and SA locate at the same binding site as the PABA-*Pa*DHPS complex. All ligands established hydrogen bonds with the sidechain of S229 and the backbone of T69, and hydrophobic interaction with the phenyl ring of F197. This agrees with previous reports that the mutations of these amino acid residues affected the binding of small molecules to DHPS.^{36, 37} This suggests that **PABA-DCM** may mimic the binding patterns of PABA to the target protein. Such similarities were also observed in the docking simulations of **PABA-DCM** and SA with DHPS from *Ec*DHPS (*Escherichia coli* dihydropteroate synthase), *Ab*DHPS

(*Acinetobacter baumannii* dihydropteroate synthase), *EfDHPS* (*Enterococcus faecalis* dihydropteroate synthase) and *SaDHPS* (*Staphylococcus aureus* dihydropteroate synthase).

Additionally, we compared the molecular docking scores of **PABA-DCM**, PABA, SA and **DCM** bound to DHPSs from 22 strains of common pathogens.^{38, 39} Specifically, PABA was used as an internal reference, and SA and **DCM** as positive and negative control, respectively. As shown in Fig. S10, no statistical difference was determined between the scoring of PABA and **PABA-DCM**, suggesting that both ligands probably bind to DHPS with similar affinity. The analysis also indicated that SA has the lowest scoring value (highest binding affinity) compared with other ligands, which is in accordance with the fact that SA is a strong competitive inhibitor of DHPS.^{40, 41} In contrast, the scoring of **DCM** is the highest among all ligands, suggesting its lowest affinity for DHPS.

Construction of PABA-DCM@GO-based hydrogel dressing. Next, we evaluated the potential for using **PABA-DCM** in the fluorescence imaging of wound-tissue infection using live mice. To facilitate wound coating, graphene oxide (GO) was used to prepare a hydrogel-based dressing of **PABA-DCM** in the presence of gelatin, a clinically common material for wound dressings. GO has been extensively shown as a promising low-dimensional material for biomedical applications including the construction of antibacterial dressings due to its intrinsic activities⁴² and the ability to enhance the stiffness of the dressing.⁴³ Through the simple self-assembly between **PABA-DCM** and GO in an aqueous solution, a **PABA-DCM@GO** ensemble was prepared.

A series of techniques were then used to characterize the ensemble. From representative transmission electronic microscopic images (Figure 6a), typical GO flakes were seen before and after assembly with

the probe. Notably, more densely clustered GO sheets were observed for **PABA-DCM@GO** than GO. Shown in Figure 6b are the representative atomic force microscopic images of GO with and without coating with **PABA-DCM**. A height increase of *ca.* 1.95 nm was observed for **PABA-DCM@GO** with respect to GO alone, suggesting the adsorption of the probes to both sides of the material surface, probably due to π - π stacking as the main driving force.²⁷ A size increase was determined for **PABA-DCM@GO** (*ca.* 296 nm) when compared to GO (*ca.* 255 nm) by dynamic light scattering (Figure 6c), and a decreased zeta potential from -25 to -34 was determined for GO after assembly with the probe (Figure 6d), suggesting an enhanced stability of the ensemble.²⁸ Finally, we used fluorescence spectroscopy to detect the fluorescence changes of the probe with GO. We observed a gradual fluorescence quenching for **PABA-DCM** with increasing concentrations of GO (Figure 6e), which agrees with results,²⁸ which suggests that the assembly of fluorescent dyes with GO can lead to fluorescence quenching due to combined mechanisms of Förster resonance energy transfer, electron transfer and inner filter effect.^{44, 45}

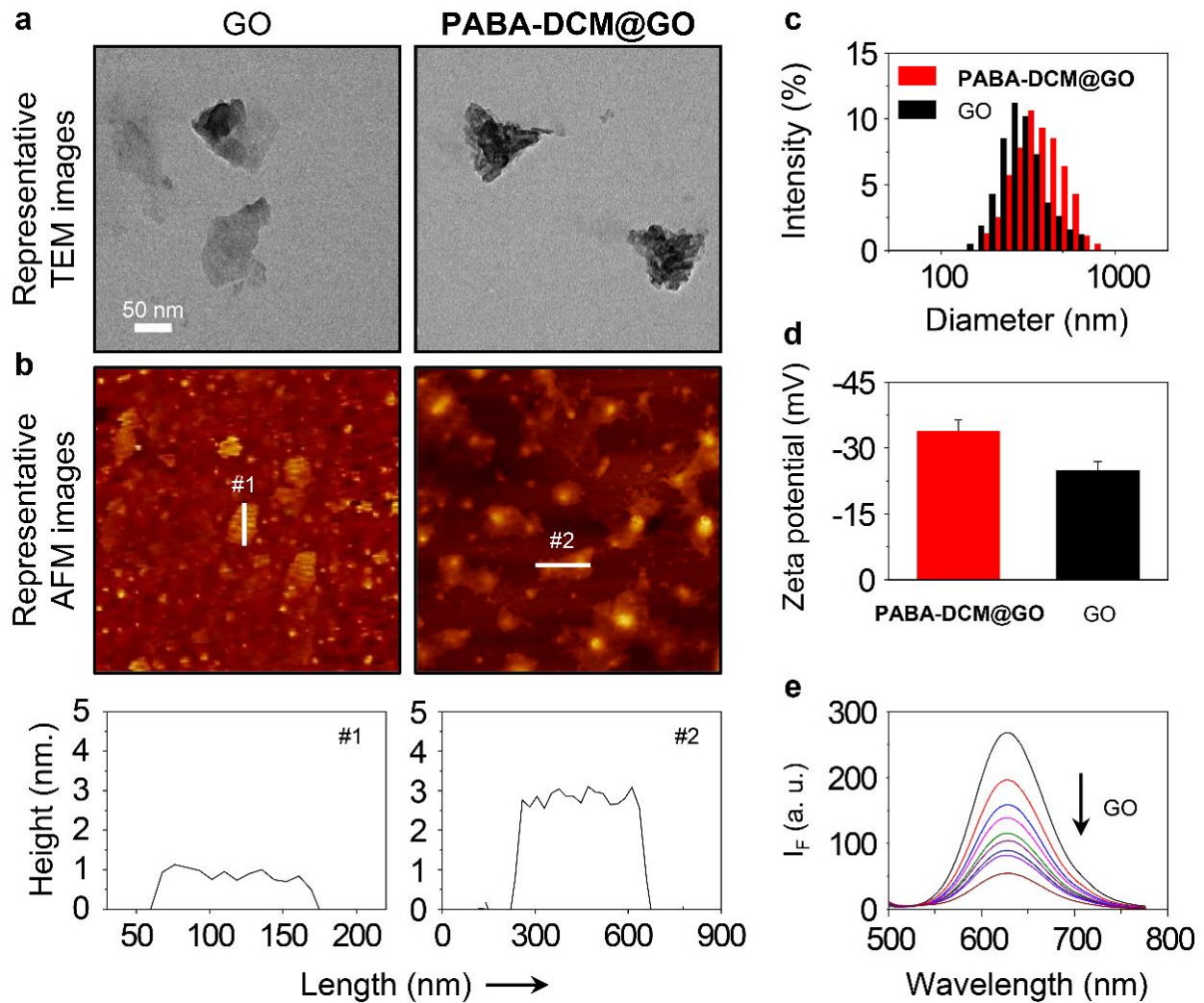


Figure 6. Characterization of PABA-DCM@GO. Representative (a) transmission electron microscopic (TEM) and (b) atomic force microscopic (AFM) images of **PABA-DCM@GO** ($\text{PABA-DCM/GO} = 1 \mu\text{M}/ 10 \mu\text{g mL}^{-1}$). (c) Dynamic light scattering and (d) zeta potential of GO ($10 \mu\text{g mL}^{-1}$) and **PABA-DCM@GO** ($\text{PABA-DCM/GO} = 1 \mu\text{M}/ 10 \mu\text{g mL}^{-1}$). (e) Fluorescence titration of **PABA-DCM** ($10 \mu\text{M}$) in the presence of increasing GO (from top to bottom curve: $0\text{-}100 \mu\text{g mL}^{-1}$) in phosphate-buffered saline solution (0.01 M , $\text{pH } 7.4$); $\lambda_{\text{ex}} = 460 \text{ nm}$.

With the **PABA-DCM@GO** ensemble in hand, we evaluated its imaging capacity for bacteria (*P. aeruginosa* ATCC 10145 and *S. aureus* ATCC 12600) and with human skin cells (HaCaT, HFF and

HMEC) as controls. We observed that analogous to **PABA-DCM**, the ensemble was amenable to fluorescence imaging of both ATCC 10145 and ATCC 12600 (Figure S11). However, minimal fluorescence was detected in the human skin cells after being treated with **PABA-DCM@GO** after 2 h (Figure S11a and S11b). Interestingly, the fluorescence intensity produced by the ensemble was stronger than that of just **PABA-DCM** in bacterial cells (Figure S11a and S11b), which agrees with our previous observation that GO enhances the imaging capacity of small-molecular fluorescent probes.⁴⁴ We also determined that the pre-incubation of PABA as a competing agent for **PABA-DCM** suppressed the fluorescence of **PABA-DCM@GO** in 5 bacterial strains (Figure S12), demonstrating that the bacterial imaging of the ensemble is also dependent on the DHPS-mediated metabolic pathway. In addition, using a series of assays including the LIVE/DEAD[®] Viability/Cytotoxicity staining (Figure S13), flow cytometry using the Annexin V-FITC/PI Apoptosis Detection Kit (Figure S14) and the CCK-8 assay (Figure S15), minimal cytotoxicity for **PABA-DCM@GO** was determined for all the skin cells evaluated.

Metabolically-selective fluorescence imaging of bacterial infection on wound tissues of mice with PABA-DCM@GO-based hydrogel dressing. We prepared a hydrogel dressing of **PABA-DCM@GO** using gelatin which facilitated the application to tissues.⁴⁶ With the hydrogel dressing prepared (Figure S16), we constructed full-thickness skin-defect wound models using male C57BL/6 mice. Circular wounds with diameter 6 mm were cut on both sides along the dorsal midline of each mouse (10 mm interval). Then, different live bacteria including *P. aeruginosa* (ATCC 10145), *E. coli* (ATCC 11775), *A. baumannii* (ATCC 19606), *E. faecalis* (ATCC 19433), and *S. aureus* (ATCC 12600) (10^6 CFU mL⁻¹) were injected sub-fascia to the left wound; the bacteria pre-treated with heat

(to induce bacterial death) (10^7 CFU mL⁻¹) were injected to the right wound of the same mice. The wound tissues were then kept soaked by wrapping with a transparent film. We observed purulent secretions on the left-infected wound for all mice groups, whereas only minimal yellow jelly-like exudations were seen on the right wound after 2 days (Figure 7a). The infection was also confirmed by the nutrient agar plating method (Figure 7a), showing a significantly larger number of bacteria on the left side than on the right. Subsequently, wounds on both sides were coated using the **PABA-DCM@GO** hydrogel dressing for 2 h, and the corresponding images were taken using a fluorescence imaging system (Figures 7b and 7c). We observed that the fluorescence intensity on the left wounded tissues (infected with live bacteria) was significantly stronger than that on the right (with heat-killed bacteria). The difference in fluorescence intensity reached up to 4-fold for the *P. aeruginosa*-infected group. These imaging results suggest that our metabolically- selective probe exhibits promise for the selective visualization of bacterial infection of wounded tissues.

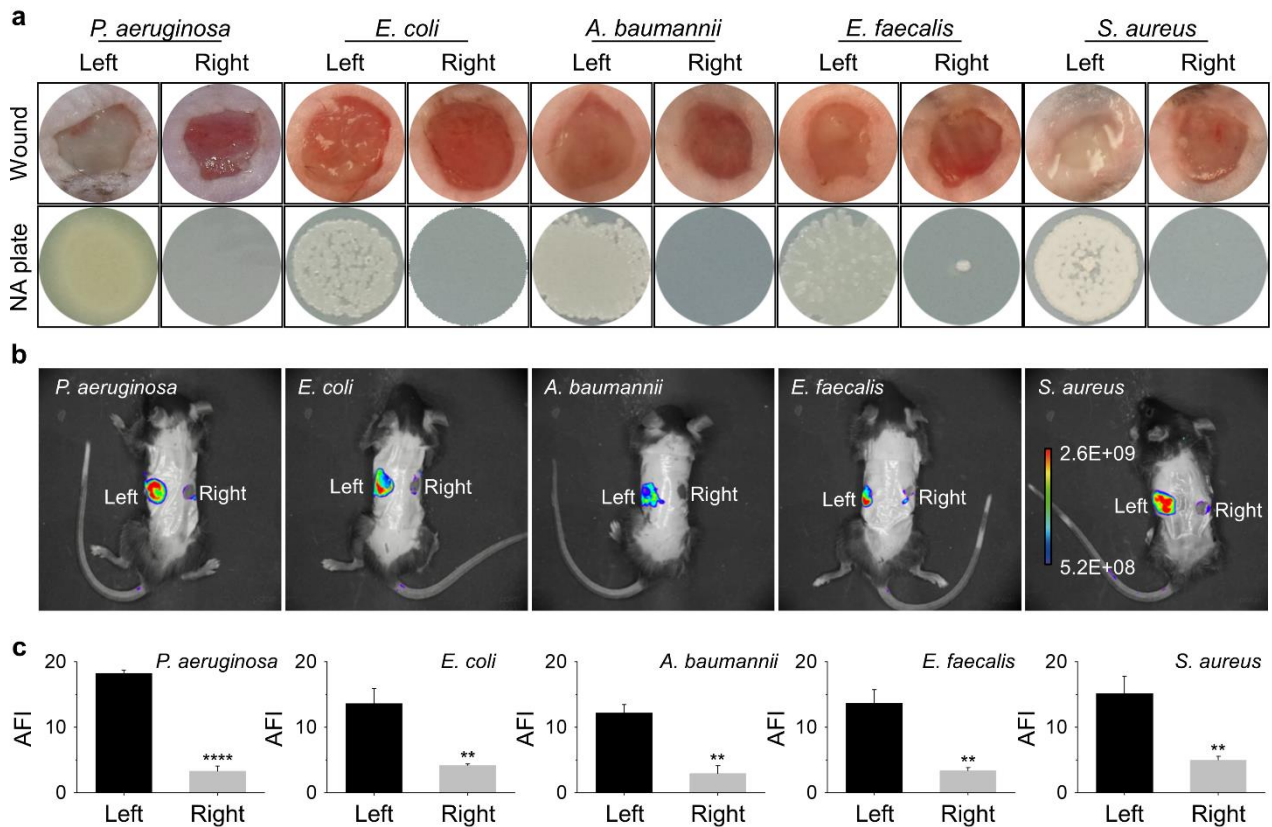


Figure 7. Metabolically-selective fluorescence imaging of infected wounds by PABA-DCM@GO with implant-related mice models. (a) Photos of wounds on both sides of implant-related mice treated with viable bacteria (10^6 CFU mL^{-1}) (left wound) and heat-killed bacteria (10^7 CFU mL^{-1}) (right wound). Wound infection was also confirmed by NA (nutrient agar) plating. (b) Fluorescence imaging of implant-related wound infection mice models treated with PABA-DCM@GO (PABA-DCM/GO = $10 \mu\text{M}/100 \mu\text{g mL}^{-1}$). The left and right wounds were infected with viable (10^6 CFU mL^{-1}) and heat-killed bacteria (10^7 CFU mL^{-1}), respectively. (c) Fluorescence quantification of the right and left wound of the mice treated with PABA-DCM@GO (PABA-DCM/GO = $10 \mu\text{M}/100 \mu\text{g mL}^{-1}$). AFI: Average fluorescence intensity ($\times 10^8$ photons/sec/cm²/sr); S.D. means standard deviation (n = 3); **P < 0.01, ****P < 0.0001.

Previously, Murawski *et al.*⁴⁷ developed a fluorine-labelled PABA analogue as a broad-spectrum imaging tracer for bacteria. However, isotopic labelling is radioactive, which poses challenges when being employed directly at the bedside. Compared to radioisotopic imaging, fluorescence is particularly advantageous in terms of biosafety, and on-demand applications since it requires a portable UV lamp and exhibits extended shelf-life. We anticipate that our **PABA-DCM@GO** hydrogel dressing with metabolic specificity for bacterial species could become a simple alternative to the current clinical methods for the effective visualization of bacterial infection *in-situ*.

Conclusions

We developed a PABA-modified long-wavelength probe, **PABA-DCM**, for the metabolically-specific imaging of bacterial species versus mammalian cells. In combination with GO, we constructed a hydrogel dressing using the probe and gelatin, thereby facilitating the *in-situ* fluorescence imaging of bacterial infections of the wounded tissues of live mice. **PABA-DCM** was shown to be specifically sequestered by the DHPS-dependent FA synthetic pathway, which is highly conserved in bacterial species, resulting in prolonged retention of the probes fluorescence. In bacteria with attenuated DHPS activity (PABA or SA inhibition) or in mammalian cells without DHPS expression, the probe was rapidly excreted. **PABA-DCM** was also shown to contribute to an increase of the FA levels in several bacteria, suggesting that the DHPS-dependent metabolism determines the prolonged retention of the probe in bacterial species. This research offers insights into the construction of imaging probes that can target pathogen-conserved metabolic pathways, making possible the development of simple and clinically transformable fluorescent agents and materials for the timely monitoring of bacterial infections *in-situ*. The development of fluorescent probes that can be activated by species-specific

biomarkers in order to further enhance imaging precision is underway in our group.⁴⁸⁻⁵² Moreover, owing to the inherent antimicrobial properties of GO, we are also exploring the use of **PABA-DCM@GO** hydrogel dressing for image-guided photodynamic and/or photothermal therapy of bacterial infections.⁵³⁻⁵⁷

ASSOCIATED CONTENT

Supporting Information. All protocols were approved by the Changhai Hospital Biosafety and the Institutional Animal Care & Use Committee of the Naval Medical University, Shanghai, China (NO. CHEC2014-096). For experimental details regarding chemical synthesis, materials characterization, fluorescence imaging in vitro and in vivo and biochemical assays, are available in the ESI. All data are expressed as mean \pm SD. The difference of multiple groups was analysed by one-factor ANOVA, followed by the SNK-q test. Statistical comparisons were carried out using SPSS Version 26. Unpaired Student's t-test was used for two groups with Prism 8 (GraphPad Software Inc.). A P value of < 0.05 was viewed as statistically significant.

AUTHOR INFORMATION

Corresponding Author

* Corresponding authors.

Zhao-Hong Chen - Department of Burn Surgery and Wound Repair, Fujian Burn Medical Center, Fujian Provincial Key Laboratory of Burn and Trauma, Fujian Medical University Union Hospital, Fuzhou 350001, Fujian, P. R. China. Email: doctorczh@163.com

Yong-Jun Zheng - Department of Burn Surgery, the First Affiliated Hospital of Naval Medical University, Shanghai 200433, P. R. China; Research Unit of key techniques for treatment of burns and combined burns and trauma injury, Chinese Academy of Medical Sciences. Email: smmuzhengyongjun@163.com

Xiao-Peng He - Key Laboratory for Advanced Materials and Joint International Research Laboratory of Precision Chemistry and Molecular Engineering, Feringa Nobel Prize Scientist Joint Research Center, School of Chemistry and Molecular Engineering, Frontiers Center for Materiobiology and Dynamic Chemistry, East China University of Science and Technology, 130 Meilong Rd, Shanghai 200237, P. R. China. Email: xphe@ecust.edu.cn

Zhao-Fan Xia - Department of Burn Surgery, the First Affiliated Hospital of Naval Medical University, Shanghai 200433, P. R. China; Research Unit of key techniques for treatment of burns and combined burns and trauma injury, Chinese Academy of Medical Sciences. Email: [xiazhaofan_smmu@163.com](mailto:xiazhaoфан_smmu@163.com)

Author Contributions

All authors have given approval to the final version of the manuscript. Chen-Jian Zhong and Xi-Le Hu performed and analysed experiments, synthesized and characterized the probes and wrote the first draft of the manuscript. Xiao-Lan Yang and Hui-Qi Gan assisted with the cell experiments. Hui-Qi Gan, Fu-Ting Shu, Pei Wei, Kai-Cheng Yan and Teng Gong contributed to the experimental investigation. Peng-Fei Luo and Tony D. James provided technical support, and helped coordinate the project, and revised the manuscript. Xiao-Peng He and Yong-Jun Zheng directed experiments and revised the

manuscript, supplemented and checked the experimental data. Zhao-Fan Xia and Zhao-Hong Chen designed and supervised the project and revised the paper.

‡These authors contributed equally.

Notes

There are no conflicts to declare.

ACKNOWLEDGMENT

This work was funded by the National Natural Science Foundation of China (91853201, 81930057, 21907030 and 82072170), the Shanghai Science and Technology Committee (No. 19410712600), CAMS Innovation Fund for Medical Sciences (2019-I2M-5-076), Achievements Supportive Fund (2018-CGPZ-B03), the Natural Science Foundation of Fujian Province (2021J01755), the 14th Five-Year Plan for Medicine and Double High Construction Project of National Clinical Key Specialty of Fujian, China ([2021]76) and Fujian Provincial Key Laboratory of Burn and Trauma, China. T.D.J. wishes to thank the Royal Society for a Wolfson Research Merit Award and the Open Research Fund of the School of Chemistry and Chemical Engineering, Henan Normal University for support (2020ZD01).

REFERENCES

(1) Allegranzi, B.; Zayed, B.; Bischoff, P.; Kubilay, N. Z.; de Jonge, S.; de Vries, F.; Gomes, S. M.; Gans, S.; Wallert, E. D.; Wu, X.; et al. New WHO recommendations on intraoperative and postoperative measures for surgical site infection prevention: an evidence-based global perspective. *Lancet Infect. Dis.* **2016**, *16*, 288-303.

- (2) Willyard, C. The drug-resistant bacteria that pose the greatest health threats. *Nature* **2017**, *543*, 15.
- (3) Haalboom, M.; Blokhuis-Arkes, M. H. E.; Beuk, R. J.; Meerwaldt, R.; Klont, R.; Schijffelen, M. J.; Bowler, P. B.; Burnet, M.; Sigl, E.; van der Palen, J. A. M. Culture results from wound biopsy versus wound swab: does it matter for the assessment of wound infection? *Clin. Microbiol. Infect.* **2019**, *25*, 7-12.
- (4) Wu, Y. K.; Cheng, N. C.; Cheng, C. M. Biofilms in Chronic Wounds: Pathogenesis and Diagnosis. *Trends Biotechnol.* **2019**, *37*, 505-517.
- (5) Wu, L.; Liu, J.; Li, P.; Tang, B.; James, T. D. Two-photon small-molecule fluorescence-based agents for sensing, imaging, and therapy within biological systems. *Chem. Soc. Rev.* **2021**, *50*, 702-734.
- (6) Zhang, Y.; Zhang, G.; Zeng, Z.; Pu, K. Activatable molecular probes for fluorescence-guided surgery, endoscopy and tissue biopsy. *Chem. Soc. Rev.* **2022**, *51*, 566-593.
- (7) Jiang, C.; Huang, H.; Kang, X.; Yang, L.; Xi, Z.; Sun, H.; Pluth, M. D.; Yi, L. NBD-based synthetic probes for sensing small molecules and proteins: design, sensing mechanisms and biological applications. *Chem. Soc. Rev.* **2021**, *50*, 7436-7495.
- (8) Lauwerends, L. J.; van Driel, P.; Baatenburg de Jong, R. J.; Hardillo, J. A. U.; Koljenovic, S.; Puppels, G.; Mezzanotte, L.; Lowik, C.; Rosenthal, E. L.; Vahrmeijer, A. L.; et al. Real-time fluorescence imaging in intraoperative decision making for cancer surgery. *Lancet Oncol.* **2021**, *22*, 186-195.
- (9) Ding, S.; Hong, Y. The fluorescence toolbox for visualizing autophagy. *Chem. Soc. Rev.* **2020**, *49*, 8354-8389.

- (10) Wang, S.; Ren, W. X.; Hou, J. T.; Won, M.; An, J.; Chen, X.; Shu, J.; Kim, J. S. Fluorescence imaging of pathophysiological microenvironments. *Chem. Soc. Rev.* **2021**, *50*, 8887-8902.
- (11) Huang, Y.; Chen, W.; Chung, J.; Yin, J.; Yoon, J. Recent progress in fluorescent probes for bacteria. *Chem. Soc. Rev.* **2021**, *50*, 7725-7744.
- (12) Wang, Z.; Xing, B. Small-molecule fluorescent probes: big future for specific bacterial labeling and infection detection. *Chem. Commun.* **2021**, *58*, 155-170.
- (13) Marshall, A. P.; Shirley, J. D.; Carlson, E. E. Enzyme-targeted fluorescent small-molecule probes for bacterial imaging. *Curr. Opin. Chem. Biol.* **2020**, *57*, 155-165.
- (14) Wang, C.; Wang, J.; Xue, K.; Xiao, M.; Wu, K.; Lv, S.; Hao, B.; Zhu, C. Polarity-Sensitive Fluorescent Probe for Reflecting the Packing Degree of Bacterial Membrane Lipids. *Anal. Chem.* **2022**, *94*, 3303-3312.
- (15) Li, L. L.; Ma, H. L.; Qi, G. B.; Zhang, D.; Yu, F.; Hu, Z.; Wang, H. Pathological-Condition-Driven Construction of Supramolecular Nanoassemblies for Bacterial Infection Detection. *Adv. Mater.* **2016**, *28*, 254-262.
- (16) Kwon, H. Y.; Liu, X.; Choi, E. G.; Lee, J. Y.; Choi, S. Y.; Kim, J. Y.; Wang, L.; Park, S. J.; Kim, B.; Lee, Y. A.; et al. Development of a Universal Fluorescent Probe for Gram-Positive Bacteria. *Angew. Chem. Int. Ed.* **2019**, *58*, 8426-8431.
- (17) Zhao, E.; Chen, Y.; Chen, S.; Deng, H.; Gui, C.; Leung, C. W.; Hong, Y.; Lam, J. W.; Tang, B. Z. A Luminogen with Aggregation-Induced Emission Characteristics for Wash-Free Bacterial Imaging, High-Throughput Antibiotics Screening and Bacterial Susceptibility Evaluation. *Adv. Mater.* **2015**, *27*, 4931-4937.

- (18) Kuru, E.; Lambert, C.; Rittichier, J.; Till, R.; Ducret, A.; Derouaux, A.; Gray, J.; Biboy, J.; Vollmer, W.; VanNieuwenhze, M.; et al. Fluorescent D-amino-acids reveal bi-cellular cell wall modifications important for *Bdellovibrio bacteriovorus* predation. *Nat. Microbiol.* **2017**, *2*, 1648-1657.
- (19) Dai, T.; Xie, J.; Zhu, Q.; Kamariza, M.; Jiang, K.; Bertozzi, C. R.; Rao, J. A Fluorogenic Trehalose Probe for Tracking Phagocytosed *Mycobacterium tuberculosis*. *J. Am. Chem. Soc.* **2020**, *142*, 15259-15264.
- (20) Mao, W.; Xia, L.; Xie, H. Detection of Carbapenemase-Producing Organisms with a Carbapenem-Based Fluorogenic Probe. *Angew. Chem. Int. Ed.* **2017**, *56*, 4468-4472.
- (21) Tian, Y.; Li, Y.; Jiang, W. L.; Zhou, D. Y.; Fei, J.; Li, C. Y. In-Situ Imaging of Azoreductase Activity in the Acute and Chronic Ulcerative Colitis Mice by a Near-Infrared Fluorescent Probe. *Anal. Chem.* **2019**, *91*, 10901-10907.
- (22) Sedgwick, A. C.; Yan, K.-C.; Mangel, D. N.; Shang, Y.; Steinbrueck, A.; Han, H.-H.; Brewster, J. T.; Hu, X.-L.; Snelson, D. W.; Lynch, V. M.; et al. Deferasirox (ExJade): An FDA-Approved AIEgen Platform with Unique Photophysical Properties. *J. Am. Chem. Soc.* **2021**, *143*, 1278-1283.
- (23) Hu, X.-L.; Sedgwick, A. C.; Mangel, D. N.; Shang, Y.; Steinbrueck, A.; Yan, K.-C.; Zhu, L.; Snelson, D. W.; Sen, S.; Chau, C. V.; et al. Tuning the Solid- and Solution-State Fluorescence of the Iron-Chelator Deferasirox. *J. Am. Chem. Soc.* **2022**, *144*, 7382-7390.
- (24) Scaranti, M.; Cojocar, E.; Banerjee, S.; Banerji, U. Exploiting the folate receptor alpha in oncology. *Nat. Rev. Clin. Oncol.* **2020**, *17*, 349-359.

- (25) Yun, M. K.; Wu, Y.; Li, Z.; Zhao, Y.; Waddell, M. B.; Ferreira, A. M.; Lee, R. E.; Bashford, D.; White, S. W. Catalysis and sulfa drug resistance in dihydropteroate synthase. *Science* **2012**, *335*, 1110-1114.
- (26) Vinnicombe, H. G.; Derrick, J. P. Dihydropteroate synthase: an old drug target revisited. *Biochem. Soc. Trans.* **1999**, *27*, 53-58.
- (27) Ji, D.-K.; Chen, G.-R.; He, X.-P.; Tian, H. Simultaneous Detection of Diverse Glycoligand-Receptor Recognitions Using a Single-Excitation, Dual-Emission Graphene Composite. *Adv. Funct. Mater.* **2015**, *25*, 3483-3487.
- (28) Ji, D. K.; Zhang, Y.; Zang, Y.; Li, J.; Chen, G. R.; He, X. P.; Tian, H. Targeted Intracellular Production of Reactive Oxygen Species by a 2D Molybdenum Disulfide Glycosheet. *Adv. Mater.* **2016**, *28*, 9356-9363.
- (29) UniProt, C. UniProt: a worldwide hub of protein knowledge. *Nucleic Acids Res.* **2019**, *47*, 506-515.
- (30) Cook, C. E.; Bergman, M. T.; Cochrane, G.; Apweiler, R.; Birney, E. The European Bioinformatics Institute in 2017: data coordination and integration. *Nucleic Acids Res.* **2018**, *46*, 21-29.
- (31) Zlitni, S.; Ferruccio, L. F.; Brown, E. D. Metabolic suppression identifies new antibacterial inhibitors under nutrient limitation. *Nat. Chem. Biol.* **2013**, *9*, 796-804.
- (32) Walsh, C. T.; Haynes, S. W.; Ames, B. D. Aminobenzoates as building blocks for natural product assembly lines. *Nat. Prod. Rep.* **2012**, *29*, 37-59.

- (33) Stratton, C. F.; Namanja-Magliano, H. A.; Cameron, S. A.; Schramm, V. L. Binding Isotope Effects for para-Aminobenzoic Acid with Dihydropteroate Synthase from *Staphylococcus aureus* and *Plasmodium falciparum*. *ACS Chem. Biol.* **2015**, *10*, 2182-2186.
- (34) Grosdidier, A.; Zoete, V.; Michielin, O. SwissDock, a protein-small molecule docking web service based on EADock DSS. *Nucleic Acids Res.* **2011**, *39*, 270-277.
- (35) Sehnal, D.; Bittrich, S.; Deshpande, M.; Svobodova, R.; Berka, K.; Bazgier, V.; Velankar, S.; Burley, S. K.; Koca, J.; Rose, A. S. Mol* Viewer: modern web app for 3D visualization and analysis of large biomolecular structures. *Nucleic Acids Res.* **2021**, *49*, 431-437.
- (36) Blair, J. M.; Webber, M. A.; Baylay, A. J.; Ogbolu, D. O.; Piddock, L. J. Molecular mechanisms of antibiotic resistance. *Nat. Rev. Microbiol.* **2015**, *13*, 42-51.
- (37) Hammoudeh, D. I.; Zhao, Y.; White, S. W.; Lee, R. E. Replacing sulfa drugs with novel DHPS inhibitors. *Future Med. Chem.* **2013**, *5*, 1331-1340.
- (38) Lachiewicz, A. M.; Hauck, C. G.; Weber, D. J.; Cairns, B. A.; van Duin, D. Bacterial Infections After Burn Injuries: Impact of Multidrug Resistance. *Clin. Infect. Dis.* **2017**, *65*, 2130-2136.
- (39) Dou, Y.; Zhang, Q. Analysis of distribution and drug resistance of pathogens of burn patients during 9 years. *Zhonghua Shao Shang Za Zhi* **2018**, *34*, 153-159.
- (40) Patel, O. G.; Mberu, E. K.; Nzila, A. M.; Macreadie, I. G. Sulfa drugs strike more than once. *Trends Parasitol.* **2004**, *20*, 1-3.
- (41) He, T.; Liu, J.; Wang, J. P. Development of a Dihydropteroate Synthase-Based Fluorescence Polarization Assay for Detection of Sulfonamides and Studying Its Recognition Mechanism. *J. Agric. Food Chem.* **2021**, *69*, 13953-13963.

- (42) Anand, A.; Unnikrishnan, B.; Wei, S. C.; Chou, C. P.; Zhang, L. Z.; Huang, C. C. Graphene oxide and carbon dots as broad-spectrum antimicrobial agents - a minireview. *Nanoscale Horiz.* **2019**, *4*, 117-137.
- (43) Shin, S. R.; Aghaei-Ghareh-Bolagh, B.; Dang, T. T.; Topkaya, S. N.; Gao, X.; Yang, S. Y.; Jung, S. M.; Oh, J. H.; Dokmeci, M. R.; Tang, X. S.; et al. Cell-laden microengineered and mechanically tunable hybrid hydrogels of gelatin and graphene oxide. *Adv. Mater.* **2013**, *25*, 6385-6391.
- (44) Lee, J.; Kim, J.; Kim, S.; Min, D. H. Biosensors based on graphene oxide and its biomedical application. *Adv. Drug Deliv. Rev.* **2016**, *105*, 275-287.
- (45) Hong, G.; Diao, S.; Antaris, A. L.; Dai, H. Carbon Nanomaterials for Biological Imaging and Nanomedicinal Therapy. *Chem. Rev.* **2015**, *115*, 10816-10906.
- (46) Buie, T.; McCune, J.; Cosgriff-Hernandez, E. Gelatin Matrices for Growth Factor Sequestration. *Trends Biotechnol.* **2020**, *38*, 546-557.
- (47) Ordonez, A. A.; Weinstein, E. A.; Bambarger, L. E.; Saini, V.; Chang, Y. S.; DeMarco, V. P.; Klunk, M. H.; Urbanowski, M. E.; Moulton, K. L.; Murawski, A. M.; et al. A Systematic Approach for Developing Bacteria-Specific Imaging Tracers. *J. Nucl. Med.* **2017**, *58*, 144-150.
- (48) Chan, H. L.; Lyu, L.; Aw, J.; Zhang, W.; Li, J.; Yang, H.-H.; Hayashi, H.; Chiba, S.; Xing, B. Unique Fluorescent Imaging Probe for Bacterial Surface Localization and Resistant Enzyme Imaging. *ACS Chem. Biol.* **2018**, *13*, 1890-1896.
- (49) Liu, T.; Yan, Q.-L.; Feng, L.; Ma, X.-C.; Tian, X.-G.; Yu, Z.-L.; Ning, J.; Huo, X.-K.; Sun, C.-P.; Wang, C.; et al. Isolation of γ -Glutamyl-Transferase Rich-Bacteria from Mouse Gut by a Near-Infrared Fluorescent Probe with Large Stokes Shift. *Anal. Chem.* **2018**, *90*, 9921-9928.

- (50) Dou, W.-T.; Qin, Z.-Y.; Li, J.; Zhou, D.-M.; He, X.-P. Self-assembled sialyllactosyl probes with aggregation-enhanced properties for ratiometric detection and blocking of influenza viruses. *Sci. Bull.* **2019**, *64*, 1902-1909.
- (51) Dou, W.-T.; Han, H.-H.; Sedgwick, A. C.; Zhu, G.-B.; Zang, Y.; Yang, X.-R.; Yoon, J.; James, T. D.; Li, J.; He, X.-P. Fluorescent probes for the detection of disease-associated biomarkers. *Sci. Bull.* **2022**, *67*, 853-878.
- (52) Dou, W.-T.; Wang, X.; Liu, T.; Zhao, S.; Liu, J.-J.; Yan, Y.; Li, J.; Zhang, C.-Y.; Sedgwick, A. C.; Tian, H.; et al. A homogeneous high-throughput array for the detection and discrimination of influenza A viruses. *Chem* **2022**, *8*, 1750-1761.
- (53) Hu, X.-L.; Chu, L.; Dong, X.; Chen, G.-R.; Tang, T.; Chen, D.; He, X.-P.; Tian, H. Multivalent Glycosheets for Double Light-Driven Therapy of Multidrug-Resistant Bacteria on Wounds. *Adv. Funct. Mater.* **2019**, *29*, 1806986.
- (54) Yu, Z.-H.; Li, X.; Xu, F.; Hu, X.-L.; Yan, J.; Kwon, N.; Chen, G.-R.; Tang, T.; Dong, X.; Mai, Y.; et al. A Supramolecular-Based Dual-Wavelength Phototherapeutic Agent with Broad-Spectrum Antimicrobial Activity Against Drug-Resistant Bacteria. *Angew. Chem. Int. Ed.* **2020**, *59*, 3658-3664.
- (55) Hu, X.-L.; Kwon, N.; Yan, K.-C.; Sedgwick, A. C.; Chen, G.-R.; He, X.-P.; James, T. D.; Yoon, J. Bio-Conjugated Advanced Materials for Targeted Disease Theranostics. *Adv. Funct. Mater.* **2020**, *30*, 1907906.
- (56) Zhang, C.; Shi, D.-T.; Yan, K.-C.; Sedgwick, A. C.; Chen, G.-R.; He, X.-P.; James, T. D.; Ye, B.; Hu, X.-L.; Chen, D. A glycoconjugate-based gold nanoparticle approach for the targeted treatment of *Pseudomonas aeruginosa* biofilms. *Nanoscale* **2020**, *12*, 23234-23240.

(57) Hu, X.-L.; Shang, Y.; Yan, K.-C.; Sedgwick, A. C.; Gan, H.-Q.; Chen, G.-R.; He, X.-P.; James, T. D.; Chen, D. Low-dimensional nanomaterials for antibacterial applications. *J. Mater. Chem. B*. **2021**, *9*, 3640-3661.

TOC picture

